JOURNAL OF MATERIALS SCIENCE **35** (2000) 3143–3149

Microstructure and mechanical properties of SiC-platelet reinforced Al_2O_3/SiC-particle hybrid composites

Y.-H. CHOA
ISIR, Osaka University, Mihogaoka 8-1, Ibaraki, Osaka 567-0047, Japan
E-mail: choa15@sanken.osaka-u.ac.jp

A. NAKAHIRA
Faculty of Engineering and Design, Kyoto Institute of Technology, Matsugasaki Sakyo-ku, Kyoto 606-8585, Japan

K. NIIHARA
ISIR, Osaka University, Mihogaoka 8-1, Ibaraki, Osaka 567-0047, Japan

SiC-platelet reinforced Al_2O_3/SiC-particle nanocomposites were fabricated by hot-pressing the mixture through the conventional powder mixing process. The mechanical properties of Al_2O_3/SiC-particle/SiC-platelet hybrid composites were evaluated. Fracture toughness and work of fracture were increased by the incorporation of SiC-platelets into Al_2O_3/SiC-particle nanocomposites. The typical rising *R*-curve was shown during crack growth for these hybrid nanocomposites, whereas Al_2O_3/SiC-particle nanocomposites showed the constant K_R value and no rising *R*-curve. The further improvement of Al_2O_3/SiC-particle nanocomposites in the creep resistance was observed by the addition of SiC platelets. The relationship between the microstructure and mechanical properties for Al_2O_3/SiC-particle/SiC-platelet hybrid composites was discussed.
© *2000 Kluwer Academic Publishers*

1. Introduction

Many studies have been reported about the use of ceramic composites for the high-temperature structural components, which demand the high fracture toughness, strength, wear resistance and deformation resistance [1–3]. In most of them, various micro meter size second phase dispersions, such as particles and whiskers, have been used [2]. These micro meter second phases were usually located at the grain boundary of matrix (these composites are named "micro-composites") and their main purpose was to increase the fracture toughness by crack deflection and/or bridging [3].

Recently much attention have been focused on ceramic nanocomposites, Al_2O_3-based, MgO-based and Si_3N_4-based nanocomposites and so on [3–6], in which the nanometer size particles, such as SiC and Si_3N_4, were dispersed mostly within the matrix grains because they possess the good mechanical properties at room temprature and high-temperature. The addition of nanometer size non-oxide ceramic particle, for example fine SiC particles, within Al_2O_3 matrix grains had been found to achieve the remarkable improvement in the fracture strength [3–6], reliability [7] and high-temperature deformation resistance (for example, creep resistance) of the Al_2O_3 matrix [8]. However, the significant increase in fracture toughness was difficult to achieve by the dispersion of nanometer size SiC particle into matrix.

One possible solution of overcoming this disadvantage is to add a third phase into nanocomposites. It was shown that the addition of reinforcement with high aspect ratio leads to a large increase in the fracture toughness, in agreement with the theoretical model [9, 10]. Whiskers, platelets and short or long fibers as the reinforcement phase are thought to be effective for producing a high performance ceramic nanocomposite. In addition, the phase transformation mechanism is attractive to obtain the tougher ceramic nanocomposites. In our previous work [11], the mechanical properties, especially toughness, of Al_2O_3/SiC-particle nanocomposites were found to be improved by the addition of ZrO_2(3Y-TZP) and SiC whiskers. However, the addition of ZrO_2 degraded the high-temperature mechanical properties. The use of SiC whisker also brings to the serious health problems, although it possesses strong potential for the achievement of good mechanical properties.

There have been many recent reports on ceramics composite reinforced by SiC platelet as a second phase. The addition of SiC platelets has a great potential for toughening the ceramic based composites. Therefore, in this study, SiC platelet was selected as the reinforcement phase for the hybrid nanocomposites. From the point of the view of high-temperature applications, the addition of SiC platelet into Al_2O_3/SiC-particle nanocomposites will be also expected to improve their

mechanical properties at high-temperature. The primary purpose of the present paper is to fabricate SiC-platelet reinforced Al_2O_3/SiC-particle nanocomposites and evaluate their mechanical properties. The second is to clarify the relationship between the microstructure and properties for the further improvement of ceramic based nanocomposites.

2. Experimental procedure

2.1. Materials fabrication

Starting powders of Al_2O_3 and SiC-particle were selected as γ-Al_2O_3 from Asahi Chemical Co. Japan and β-SiC from Ibiden Co. Japan. The average particle size of γ-Al_2O_3 and β-SiC were approximately 25 nm and below 100 nm, respectively. SiC platelet as the reinforcement phase was α-SiC single crystals from C-axis Corp. Canada, 10–20 μm in diameter and 3–6 μm in thickness. One composition, containing 17vol%SiC-particle, was chosen for the Al_2O_3/SiC-particle nanocomposites in this study. The mixture of Al_2O_3/17vol%SiC-particle was ball-milled in ethanol with Al_2O_3 balls for 12 h and then 20vol% SiC platelet was added into the mixture. This slurry was again wet-ball milled for 6 h. The slurry was completely dried by microwave and then mixed by dry-ball milling with Al_2O_3 ball for 6 h. The mixed powder of Al_2O_3/SiC-particle/SiC-plate was hot-pressed at 1600 to 2000 °C in N_2 atmosphere with an applied pressure of 30 MPa. In the present study, monolithic Al_2O_3 and Al_2O_3/SiC-particle nanocomposite was fabricated for comparison with the Al_2O_3/SiC-particle/SiC-platelet hybrid composites.

2.2. Mechanical testing and observation

The hot-pressed samples were ground with #400 diamond wheel and cut with a diamond blade into rectangular bars ($3 \times 4 \times 36$ mm). The tensile surface of all bend specimens was perpendicular to the hot-pressing axis. The edges of specimen were beveled. The density was determined using Archimedes displacement method in toluene. Young's modulus was measured by resonance-vibration method [12] as follows. The specimens were coated by a carbon paint on one side in order to act as an electrode and then suspended on two thin tungsten wires in correspondence of the nodal points. Flexural vibrations were generated by electrostatic force and reasonance frequencies were determined by using an oscilloscope. Young's modulus, E was calculated by using the following equation:

$$E = \frac{0.9468\left(L^3 P f_0^2\right)}{\left(d^3 w\right)} \tag{1}$$

where L is the length of the specimen, d is the thickness, w is the width, P is the weight and f_0 is the resonance frequency.

Hardness values were determined using Vickers indentation on the polished surface perpendicular to the hot-pressing axis with a load of 98 N. Fracture toughness was measured using two methods: the indentation method (IM) and chevron-notch beam (CN) method.

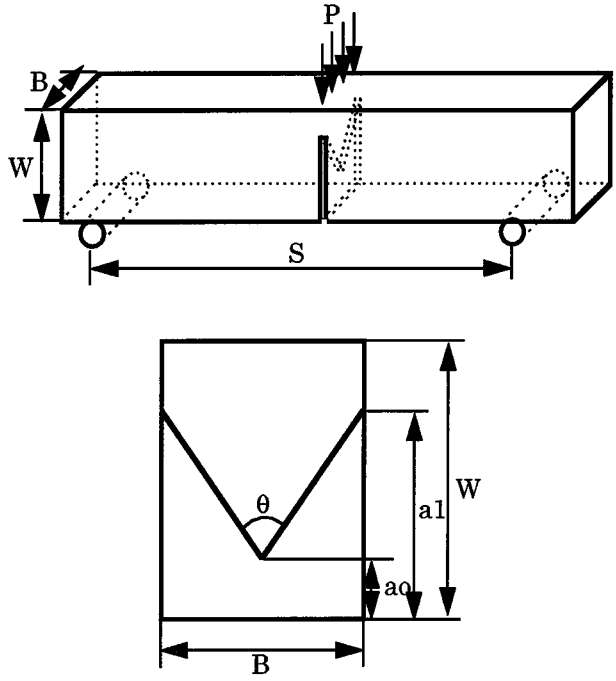

Figure 1 Schematic drawing of a CN specimen.

For the former method, the indentation load of 98 N was applied for 15 s and the fracture toughness, K_{IC} values were calculated by using be following empirical equation for median crack [13].

$$\frac{K_{IC}}{H_v a^{\frac{1}{2}}} = 0.203\left(\frac{c}{a}\right)^{\frac{-3}{2}} \tag{2}$$

where c and a are the lengths of median crack and half of the diagnoal of the indentation, respectively. Indentation with a load of 98 N was carried out on the polished surface perpendicular to the hot-pressing axis. The Chevron-notch was cut with a thin diamond blade (slot 150 μm), as shown in Fig. 1: $a_0 = 2.2$ mm and $a_1 = 3.6$ mm. The ligament area of CN specimen was approximately 3.3 mm^2. Fracture energy and R-curve behavior were also measured by CN method at the crosshead speed of 0.005 mm/min and calculated from the load-displacement curve.

The intensity factor, K_I, can be determined from the CN method using Bluhm's synthesized numerical slice model [14] as follows:

$$K_I = \left[\left(\frac{E'}{2B}\right)\left(\frac{d\lambda}{d\alpha}\right)\right]^{\frac{1}{2}} P \tag{3}$$

where λ is the dimensionless compliance, $\alpha = a/W$ is the crack length related to the width W, P is the load, E' is the elasticity for the plane strain condition. The crack length corresponding to a load can also be calculated from the change in specimen compliance. Then, the variation of fracture resistance with crack extension thus can be obtained.

The K_{IC} value was calculated at, P_{max}, the top of the load-displacement curve, from which the K_R values for the successive crack extension (rising R-curve behavior) were also obtained.

The work of fracture was calculated by integrating the load-displacement curve and dividing by twice the fractured area (Equation 4). For comparison, K_{IC} values were also calculated from the work of fracture using Irwin's similarity Equation 5 [15] (i.e. under the assumption of the perfectly linear elastic material.). In the calculation, the Young's modulus as calculated by Equation 1 was used.

$$\gamma_{\text{eff}} = \frac{W_{\text{WOF}}}{2A} \tag{4}$$

$$K_{\text{I}} = (2E'\gamma_{\text{eff}})^{\frac{1}{2}} \tag{5}$$

where W_{WOF} is the energy under the load-displacement curve, and A is the area of the specimen web portion.

Fracture strength test was carried out in three-point bending (span of 30 mm) at the crosshead speed of 0.5 mm/min. The creep test was performed in air atmosphere at 1300 °C by four-point bending test (4PBT; inner span of 10 mm and outer span of 30 mm) with an applied stress of 10 to 200 MPa as following by designation: JIS-R1612).

The composition of the hot-pressed specimens was analyzed by X-ray diffraction with Cu-K_α radiation. Microstructure was observed by optical microscopy, scanning electron microscopy (SEM) and transmission electron microscopy (TEM). The observation of fracture surface after mechanical testing was done by SEM. Polished surfaces of specimens were thermally etched in vacuum and the grain size of the Al_2O_3 matrix was determined by the intercept method [16] on the etched composites.

3. Results and discussion

3.1. Microstructure

The results of X-ray diffraction analysis indicated that the components of all sintered specimens of Al_2O_3/SiC-particle/SiC-platelet hybrid composites were α-Al_2O_3, β-SiC particle and α-SiC platelet without any reaction phases. Fig. 2 shows the optical micrograph of Al_2O_3/SiC-particle/SiC-platelet hybrid composites hot-pressed at 1900°C. SiC platelets were homogeneously dispersed in Al_2O_3 matrix and their agglomeration was not observed by the optical microscopy. TEM observation showed that nano-sized SiC particles were dispersed in the Al_2O_3 matrix grains and the SiC platelets were dispersed at the grain boundary of Al_2O_3 matrix for the Al_2O_3/SiC-particle/SiC-platelet hybrid composites, as shown in Fig. 3. Furthermore,

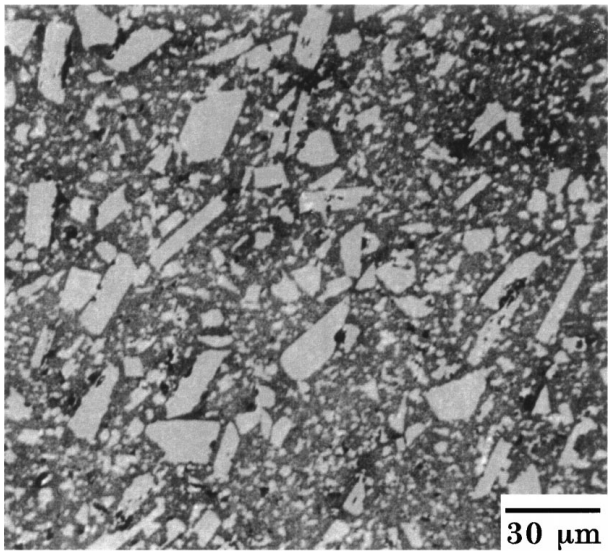

Figure 2 Optical micrograph of Al_2O_3/SiC-particle/SiC-platelet composite. Photograph showed the surface perpendicular to the pressing direction of hot-pressing.

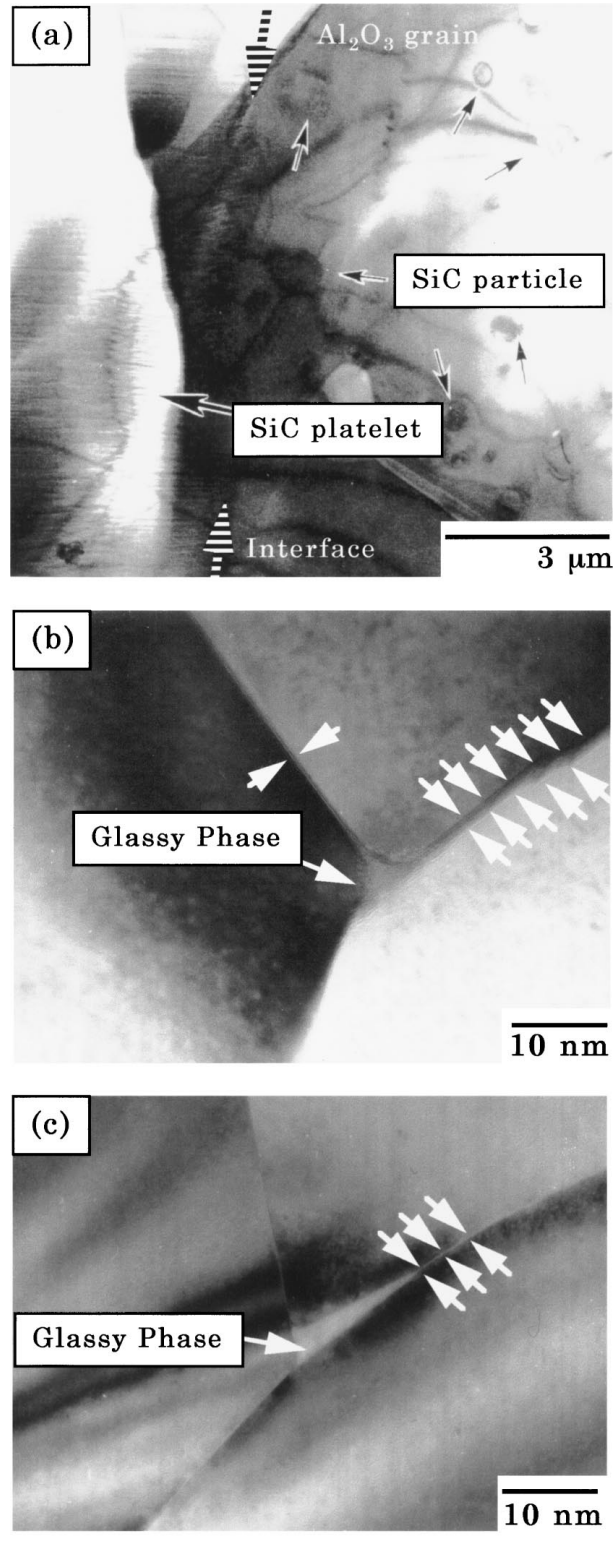

Figure 3 Transmission electron micrograph of (a) low magnification and (b) the Al_2O_3/Al_2O_3 grain boundary structure for Al_2O_3/SiC-particle/SiC-platelet composites, and (c) the Al_2O_3/Al_2O_3 grain boundary structure for monolithic Al_2O_3.

little glassy phase and reaction phase between the SiC-platelets and the Al_2O_3 matrix was observed by TEM for the Al_2O_3/SiC-particle/SiC-platelet hybrid composites.

Recent work by Ohji *et al.* [8] demonstrated a good example of direct bonding of Al_2O_3/SiC interface for Al_2O_3/SiC-particle nanocomposites, which is explained by the factors determining the equilibrium thickness of glassy film, the combination of internal thermal force and the forces of van der Waals, structural disjoining, capillary and applied forces. The attractive van der Waals force arising at the Al_2O_3/SiC interfaces was greater than that at the Al_2O_3/Al_2O_3 interfaces. This high van der Waals force plus the externally applied force with accompanying the hot-pressing (at least 30 MPa) and the internal thermal force (due to thermal expansion mismatch between the Al_2O_3 and SiC during the cooling down process) overcome the structural disjoining force and removed glassy films at most of the Al_2O_3/SiC interfaces. Thus, it is believed that the Al_2O_3/SiC interfaces were almost free from glassy phase and reaction phase as observed in the TEM observation in this study. Furthermore, the Al_2O_3/SiC interfaces were more rigid, which was due to residual stress generated by thermal expansion mismatch during the cooling down process, than Al_2O_3/Al_2O_3 grain boundary. On the other hand, large amount of glassy phase which due to the impurities and SiO_2 from the surface oxygen of SiC particles and platelets were observed in the triple junction and even the grain boundaries for the Al_2O_3/SiC-particle/SiC-platelet composites (Fig. 3b), while the glassy film in the monolithic Al_2O_3 was almost observed in the triple junction of Al_2O_3 grains and thin layer between the Al_2O_3 grain boundaries (Fig. 3c).

The dependence of hot-pressing temperature on the density of Al_2O_3/SiC-particle/SiC-platelet hybrid composites is shown in Fig. 4. The density of Al_2O_3/SiC-particle/SiC-platelet hybrid composites hot-pressed at 1800 °C was nearly 98% of the theoretical density. Fully dense Al_2O_3/SiC-particle/SiC-platelet hybrid composites were farbicated at hot-pressing temperature >1900 °C. However, in previous studies [3–5], Al_2O_3/SiC-particle nanocomposites with 17–33 vol% of SiC volume showed the almost full density (over 99% of the theoretical density) when hot-pressed at 1800 °C, so the densification of Al_2O_3 matrix was found to be significantly inhibited by the addition of SiC platelets due to the difficulty of particle rearrangements in the initial stage in sintering, similar to whisker reinforced composites.

The results of SEM observation of etched surfaces showed that grain size of Al_2O_3 matrix grain of Al_2O_3/SiC-particle/SiC-platelet hybrid composites hot-pressed at 1800 °C was approximately 2 μm. On the other hand, Al_2O_3/SiC-particle nanocomposites hot-pressed at 1800 °C showed a grain size of approximately 2.5 μm for the Al_2O_3 matrix. Monolithic Al_2O_3 hot-pressed at 1800 °C was composed of equi-axis grain of 22 μm. Therefore, these results suggested that the addition of nanometer size SiC particle and SiC-platelet have the significant role on the inhibition of densification and the grain growth in the Al_2O_3 matrix.

3.2. Mechanical properties

Vickers hardness (Hv) and Young's modulus (E) of Al_2O_3/SiC-particle/SiC-platelet hybrid composites with hot pressing temperature are shown in Fig. 5. Hv and E are 18.5 GPa and 370 GPa for monolithic Al_2O_3 and 22 GPa and 383 GPa for Al_2O_3/SiC-particle nanocomposites, respectively.

The addition of SiC platelets into Al_2O_3/SiC-particle nanocomposites increased the hardness and Young's modulus. Al_2O_3/SiC-particle/SiC-platelet hybrid composites had the constant and maximum hardness value (25 GPa) and Young's modulus (400 GPa) at hot-pressing temperature >1900 °C, which was in good agreement to that expected by the rule of mixtures with the SiC volume fraction.

Fig. 6 shows the effect of hot-pressing temperature on toughness of Al_2O_3/SiC-particle/SiC-platelet composites by the IM method. Fracture toughness of monolithic Al_2O_3 and Al_2O_3/SiC-particle nanocomposites were 3.2 MPa $m^{1/2}$ and 4.6 MPa $m^{1/2}$ respectively. Fracture toughness of Al_2O_3/SiC-particle/SiC-platelet composites increased with hot-pressing temperature. The lower fracture toughness of Al_2O_3/SiC-particle/SiC-platelet hybrid composites hot-pressed below 1850 °C

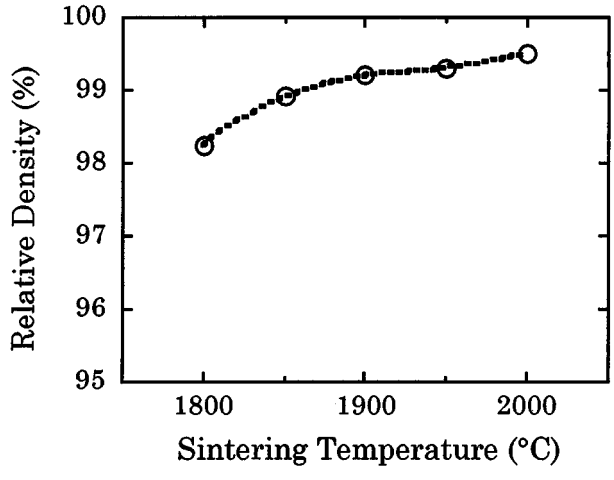

Figure 4 Variation of density of Al_2O_3/SiC-particle/SiC-platelet hybrid composites with the hot-pressing temperature.

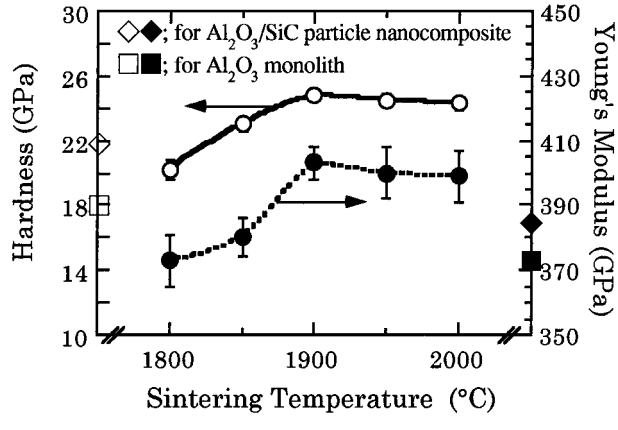

Figure 5 Variation of hardness and Young's modulus of Al_2O_3/SiC-particle/SiC-platelet hybrid composites with the hot-pressing temperature.

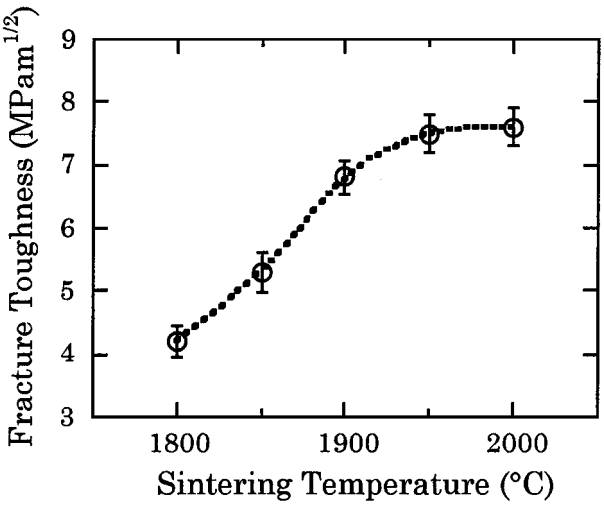

Figure 6 Variation of fracture toughness of Al_2O_3/SiC-particle/SiC-platelet hybrid composites with the hot-pressing temperature by IM method.

was caused by the presence of pores in the sintered bodies. Above 1900 °C of hot-pressing temperature, fracture toughness was the almost constant value of 7.5 MPa $m^{1/2}$. Al_2O_3/SiC-particle/SiC-platelet hybrid composites exhibited up to a 90% increase in fracture toughness, when compared to Al_2O_3/SiC-particle nanocomposite. Some researchers reported that the addition of SiC platelet showed a large increase in fracture toughness of Si_3N_4 [17] and Al_2O_3 [18]. The toughening mechanism in this hybrid materials, therefore, is thought to be the crack deflection and/or bridging by the SiC platelets.

The above-mentioned results suggest that the optimum hot-pressing temperatures were considered to be at 1900 °C for Al_2O_3/SiC-particle/SiC-platelet hybrid composites. Therefore, the following mechanical tests were done mainly for the specimens hot-pressed at 1900 °C.

CN tests were done for monolithic Al_2O_3 hot-pressed at 1500 °C, Al_2O_3/SiC-particle nanocomposites hot-pressed at 1600 °C and Al_2O_3/SiC-particle/SiC-platelet hybrid composites hot-pressed at 1900 °C. The fracture toughness by CN method was calculated from the maximum load in the load-displacement curve. For comparison, K_{IC} values were also calculated from the work of fracture. The fracture toughness and work of fracture are summarized in Table I. Al_2O_3/SiC-particle/SiC-platelet hybrid composites showed an improvement in fracture toughness over 2 times of monolithic Al_2O_3. However, the fracture toughness of hybrid composite measured by CN test shows significantly different value, 5.8 MPa $m^{1/2}$ from that of IM method.

TABLE I Fracture toughness, K_{IC} and work of fracture, γ_{eff} for monolithic Al_2O_3, Al_2O_3/SiC particle nanocomposite and Al_2O_3/SiC-particle/SiC-platelet hybrid composites

		K_{IC} (MPa $m^{1/2}$)		
	γ_{eff} (J/m^2)	IM method	CN method	By Irwin's eq
Monolithic Al_2O_3	11.2	3.2	3.1	2.9
Al_2O_3/SiC-particle nanocomposite	15.2	4.6	4.4	3.5
Al_2O_3/SiC particle-SiC platelet composite	82.2	7.5	5.8	8.3

Generally, the materials with rising *R*-curve, the evaluation of K_{IC} by CN test was not available [19], because the maximum load, P_{max}, does not occur at minimum crack length related to the width, α_{min}. The P_{max} at α_{min} is necessary value for the calculation of K_{IC}. On the other hand, for the Al_2O_3/SiC-particle nanocomposites and monolithic Al_2O_3 which shows flat *R*-curve, the K_{IC} values measured by CN test well agreed to those by IM method.

Furthermore, the work of fracture of Al_2O_3/SiC-particle/SiC-platelet hybrid composites was significantly larger than those of monolithic Al_2O_3 and Al_2O_3/SiC-particle nanocomposites. The addition of SiC-platelets was found to be significantly effective in the improvement of fracture resistance and the work of fracture of Al_2O_3/SiC-particle nanocomposites. Fig. 7 shows the fracture surface after the CN test for Al_2O_3/SiC-particle/SiC-platelet composite, monolithic Al_2O_3 and Al_2O_3/SiC-particle nanocomposites. Al_2O_3/SiC-particle/SiC-platelet hybrid composites show the rough surface of intergranular SiC-platelet and intragranular surface of Al_2O_3 matrix. On the other hand, the fracture of monolithic Al_2O_3 was mainly the intergranular mode, whereas Al_2O_3/SiC-particle nanocomposites shows the intragranular fracture of Al_2O_3 matrix.

Fig. 8 shows K_R curves of monolithic Al_2O_3 hot-pressed at 1500 °C, Al_2O_3/SiC-particle nanocomposites hot-pressed at 1600 °C and Al_2O_3/SiC-particle/SiC-platelet hybrid composites hot-pressed at 1900 °C. Al_2O_3/SiC-particle/ SiC-platelet hybrid composites indicated a typical rising *R*-curve and their K_R increased from 5.7 to a maximum K_R value of 8.5 MPa $m^{1/2}$. Monolithic Al_2O_3 had also a slightly rising *R*-curve, whereas Al_2O_3/SiC-particle nanocomposites showed the constant K_R values and no rising-*R*-curve. This slight increase in K_R of monolithic Al_2O_3 was caused by the grain bridging of Al_2O_3 matrix grains as understood by intergranular fracture as shown in Fig. 7a.

On the other hand, for the Al_2O_3/SiC-particle nanocomposites with flat *R*-curve, steeply rising *R*-curve behavior due to the nano-sized particles and intraganular fracture shown in Fig. 7b was considered in a several-nanometer-range rather than micrometer-range [20]. Therefore, the effect of nanometer size particles is thought to be too small to show the rising *R*-curve behaviors in the CN test (for this test, the evaluation of the *R*-curve is for long crack resistance in the region of several hundred μm), because of their little effect of long-crack bridging.

The great increase in fracture resistance and work of fracture for Al_2O_3/SiC-particle/SiC-platelet hybrid composites was contributed mainly by the brdiging of SiC-platelets shown in Fig. 7c and in part nanometer size SiC particles. Therefore, the addition of SiC-platelets was found to be greatly effective for toughening the Al_2O_3/SiC-particle nanocomposites.

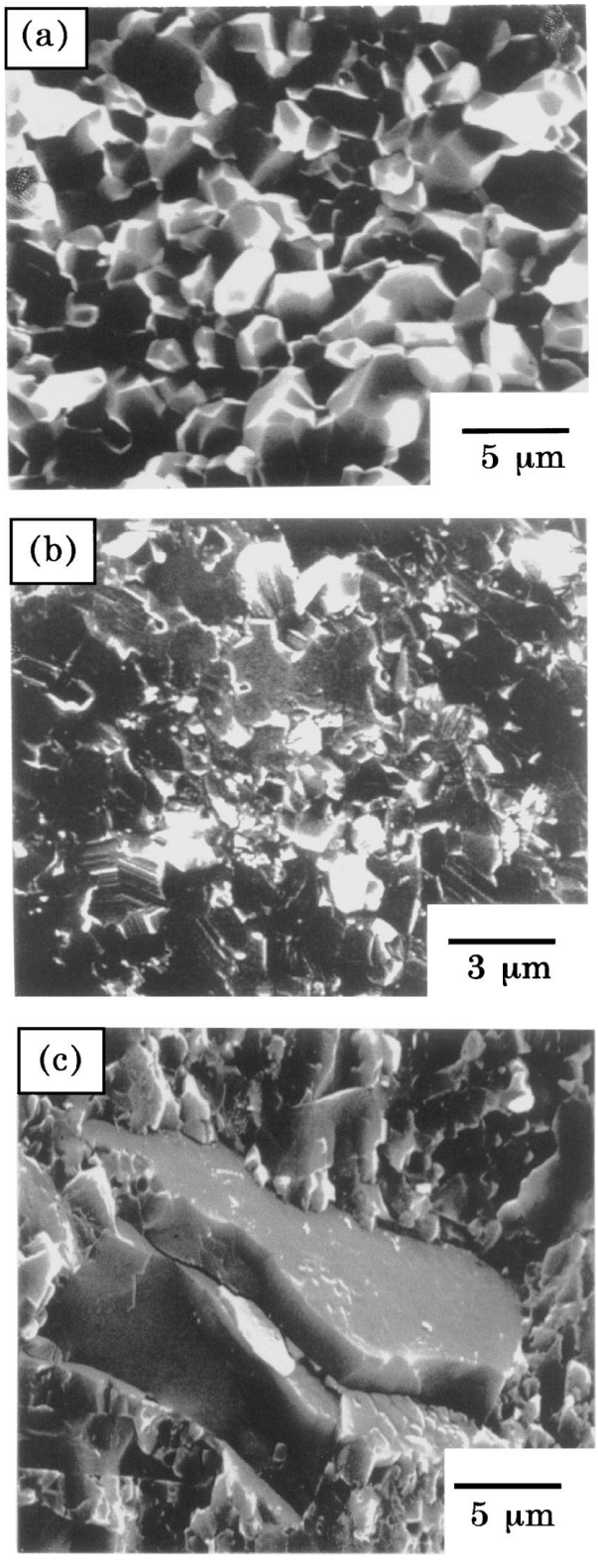

Figure 7 Scanning electron micrograph of fracture surface of ligament after CN test: (a) monolithic Al_2O_3, (b) Al_2O_3/SiC-particle nanocomposite, and (c) Al_2O_3/SiC-particle/SiC-platelet composite.

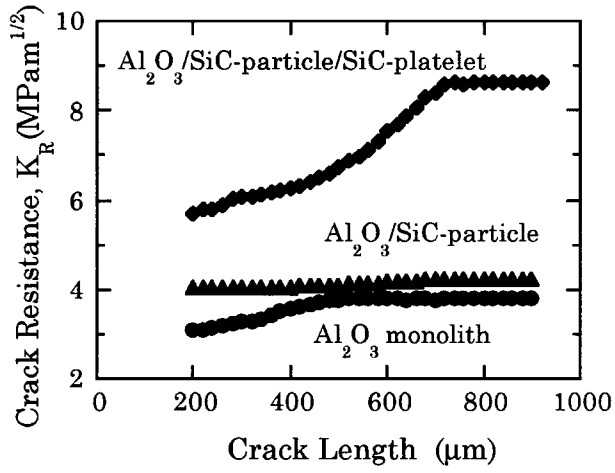

Figure 8 Variation of crack resistance, K_R of monolithic Al_2O_3, Al_2O_3/SiC-particle nanocomposite, and Al_2O_3/SiC-particle/SiC-platelet hybrid composites with the crack growth by CN method.

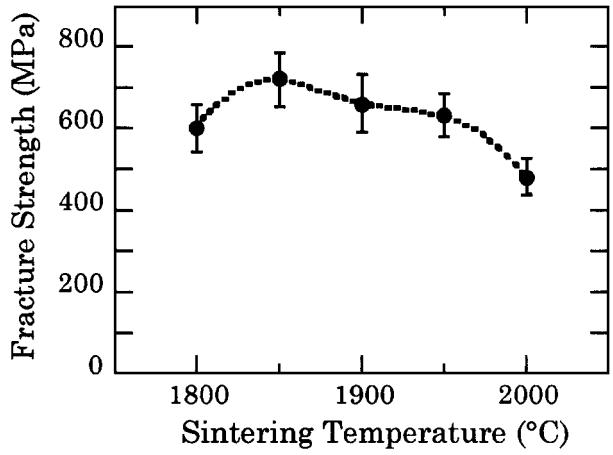

Figure 9 Variation of fracture strength of Al_2O_3/SiC-particle/SiC-platelet hybrid composites with the hot-pressing temperature.

Variation of fracture strength of Al_2O_3/SiC-particle/SiC-platelet hybrid composites with hot-pressing temperature is shown in Fig. 9. The maximum strength of 700 MPa was achieved for Al_2O_3/SiC-particle/SiC-platelet composite hot-pressed at 1900 °C. According to the results by Chou and Green [21], the strength of Al_2O_3/SiC-platelet composites hot-pressed was about 500 MPa (when the same grade of SiC platelet was used.) This high strength of Al_2O_3/SiC-particle/SiC-platelet composite was contributed to both the fine microstructure produced by the nanometer size SiC particle and the increase in fracture resistance.

The creep test at 1300 °C was done for monolithic Al_2O_3 hot-pressed at 1500 °C, Al_2O_3/SiC-particle nanocomposites hot-pressed at 1600 °C and Al_2O_3/SiC-particle/SiC-platelet hybrid composites hot-pressed at 1900 °C. Fig. 10 indicates the variation of strain rate with applied stress. The creep rate of the nanocomposites was about three orders of magnitude lower than that of monolithic Al_2O_3. Further improvement of creep resistance was obtained by the simultaneous addition of SiC-platelets and SiC particles. These results of the creep tests suggest that the creep resistance were mainly improved by the addition of the nano-sized SiC particles.

The SiC nano-particle is thought to have two roles; 1) some intergranular SiC particles at the grain boundaries at the Al_2O_3 matrix reduce the diffusion creep rate and, as a result, inhibit the grain boundary sliding [8], and 2) the intragranular SiC particle inhibit the dislocation movement and growth of microcavity, which could be effective at high-applied pressure and high temperature which the dislocations mainly controlled

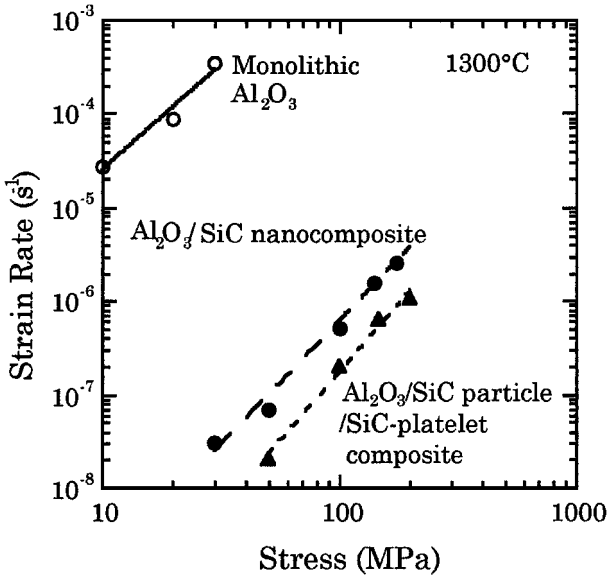

Figure 10 Stress dependency of strain rate of monolithic Al_2O_3, Al_2O_3/SiC-particle nanocomposite, and Al_2O_3/SiC-particle/SiC-platelet hybrid composites by 4PBT.

the creep role. Because grain boundary diffusion is the most predominant deformation mechanism of alumina polycrystalline at the temperature around 1200–1300°C, the dominant effect for the improvement of the creep resistance should be inhibition of grain boundary sliding. Further inhibition of grain boundary sliding was obtained by the simultaneous addition of SiC-platelets and SiC particles.

Raj and Ashby calculated the sliding rate with diffusional accommodation when secondary particles are present on the grain boundaries and showed that creep is not slowed if the diffusivity of the particle-matrix interfaces is equivalent to that of matrix-matrix interface [22]. However, it is reported that the diffusion ability in the alumina/silicon carbide interface of nanocomposites is significantly lower than that in alumina/alumina grain boundary [8]. This lower diffusivity was attributed to the rigid and clean interface of alumina/silicon carbide, as discussed in previous part. This fact was also easily understood from lower sinterability of composites than monolithic alumina.

4. Conclusion

SiC-platelet reinforced Al_2O_3/SiC-particle nanocomposites were achieved by the hot-pressing the mixture of Al_2O_3, SiC-particle and SiC-platelet. The microstructure and mechanical properties were evaluated for Al_2O_3/SiC-particle/SiC-platelet hybrid composites.

1. Fully dense Al_2O_3/SiC-particle/SiC-platelet hybrid composites were successfully fabricated by hot-pressing, and their microstructure showed that the Al_2O_3/SiC interface was clean and rigid due to residual stress, whereas the Al_2O_3/Al_2O_3 grain boundary with large amount of glassy phase also detected due to an impurity and surface silicon oxide from starting SiC materials.

2. Fracture toughness and work of fracture of Al_2O_3/SiC-particle nanocomposites were improved by the addition of the SiC-platelets. The increase in fracture toughness and work of fracture for Al_2O_3/SiC-particle/SiC-platelet hybrid composites was thought to be due to the bridging by SiC-platelets.

3. The addition of SiC-platelet into Al_2O_3/SiC-particle nanocomposites resulted in a rising *R*-curve behavior, whereas Al_2O_3/SiC-particle nanocomposites showed the constant K_R value and no rising *R*-curve. The K_R increased from 5.7 to a maximum value of 8.5 MPa $m^{1/2}$. The strength of Al_2O_3/SiC-particle/ SiC-platelet hybrid composites was approximately 700 MPa.

4. The creep resistance of Al_2O_3/SiC-particle nanocomposites was improved by the addition of SiC-platelets. The SiC-platelets is to inhibit the grain boundary sliding of Al_2O_3 matrix in addition to that of nanosized SiC particles. It is due to the more rigid and clean interface of the Al_2O_3/SiC than the grain boundary of alumina/alumina.

References

1. J. R. PORTER, F. F. LANGE and A. H. CHOKSKI, *Am. Ceram. Soc. Bull.* **66** (1987) 343.
2. N. CLAUSSEN, J. STEEB and R. F. PABST, *ibid.* **56** (1977) 559.
3. K. NIIHARA, A. NAKAHIRA, T. UCHIYAMA and T. HIRAI, in "Fracture Mechanics of Ceramics, Vol. 7," edited by R. C. Bradt, A. G. Evans, D. P. H. Hasselman and F. F. Lange (Plenum Press, New York, 1986) p. 103.
4. K. NIIHARA, *J. Ceram. Soc. Jpn.* **99** (1991) 974.
5. A. NAKAHIRA and K. NIIHARA, in Fracture Mechanics of Ceramics, Vol. 9, Ed. by M. Sakai, R. C. Bradt, D. P. H. Hasselman and D. Munz (Plenum Press, New York, 1992) p. 165.
6. T. HIRANO and K. NIIHARA, *Nanostruct. Mater.* **5** (1995) 808.
7. A. NAKAHIRA, PhD thesis, Osaka University, 1992.
8. T. OHJI, T. HIRANO, A. NAKAHIRA and K. NIIHARA, *J. Am. Ceram. Soc.* **79** (1996) 35.
9. K. T. FABER and A. G. EVANS, *Acta Metall.* **31** (1983) 565.
10. *Idem., ibid.* **31** (1983) 577.
11. S. INOUE, T. UCHIYAMA and K. NIIHARA, *J. Jpn. Soc. Powder and Powder Metall.* **37** (1990) 341.
12. K. MATSUSHITA, S. KURATANI, T. OKAMOTO and M. SHIMADA, *J. Mater. Sci. Lett.* **3** (1984) 345.
13. K. NIIHARA, R. MORENA and D. P. H. HASSELMAN, *ibid.* **1** (1982) 13.
14. J. I. BLUHM, *Eng. Fract. Mecha.* **7** (1975) 593.
15. G. R. IRWIN, *J. Appl. Mech.* **24** (1957) 361.
16. J. C. VANLOON and C. M. PARISSIS, *Analyst.* **94** (1969) 1057–1062.
17. N. CLAUSSEN, in the Proceedings of the 11 RISO International Symposium on Metallugy and Materials Science, Structural Ceramics Processing, Microstructure and Properties, edited by J. J. Bentzen, J. B. Blide-Soresen, N. Christiansen, A. Horsewell and B. Ralph (RISO National University, Denmark, 1990) p. 1.
18. G. SANDERS and M. V. SWAIN, *Mater. Forum.* **14** (1990) 60.
19. D. MUNZ, in "Fracture Mechanics of Ceramics, Measurements, Transformations, and High Temperature Fracture, Vol. 6," edited by R. C. Bradit, A. G. Evans, D. P. H. Hasselman and F. F. Lange (Plenum Press, New York, 1983) p. 1.
20. T. OHJI, Y. K. JEONG, Y.-H. CHOA and K. NIIHARA, *J. Am. Ceram. Soc.* **81** (1998) 1453.
21. Y. S. CHOU and D. J. GREEN, *ibid.* **76** (1993) 1452.
22. R. RAJ and M. F. ASHBY, *Metall. Trans.* **2** (1971) 1113.

Received 24 August
and accepted 20 December 1999